Assiut University Journal of Multidisciplinary Scientific Research (AUNJMSR)
Faculty of Science, Assiut University, Assiut, Egypt.
Printed ISSN 2812-5029
Online ISSN 2812-5037
Vol. 53(2): 335- 348 (2024)
https://aunj.journals.ekb.eg

Barium incorporated zirconium dioxide nanostructures synthesized by sol-gel route and investigation of their structural, thermal and spectroscopic characteristic in the stabilized tetragonal phase

Abdulaziz Abu El-Fadl[1,2], A. A. Abu-Sehly[1,2] and Rania A. El-Touny *[2]

[1]Physics Department, Faculty of Science, Assiut University, 71516 Assiut, Egypt
[2]Lab. of Smart Materials for Energy Futures, Physics Department, Faculty of Science, Assiut University, 71516 Assiut, Egypt

*Corresponding Author: Rania Touny; Email: a_rania49@yahoo.com

ARTICLE INFO

Article History:
Received: 2024-03-20
Accepted: 2024-04-21
Online: 2024-04-29

Keywords:
Ba-doped ZrO_2, Nanomaterials, Sol-gel process, Optical properties.

ABSTRACT

Zirconium dioxide (ZrO_2) is one of the hypothetical ceramic materials, which exhibits appealing thermal, mechanical, electrical, and optical qualities as well as strong oxygen ion conductivity. In this work, ZrO_2 nanostructure doped with various Barium ratios using a sol-gel approach was successfully prepared. The impact of increasing the percentage of barium integrated in zirconium dioxide (Ba_xZrO_2) (the weight percentages are x = 1%, 2%, 5%, 6%, 8%, and 10%) on the temperature at which a tetragonal phase form was examined. X-ray diffraction (XRD) was utilized to identify the structure of the prepared samples. XRD patterns showed that the incorporation of Ba into the ZrO_2 lattice stabilized the tetragonal phase up to 900 °C. Fourier transform infrared spectroscopy (FTIR) was used to analyze the phase composition, while differential scanning calorimetry (DSC) was employed to study and validate the thermal analysis. Furthermore, images obtained using a scanning electron microscope (SEM) depict the surface morphology of the prepared specimens. To find the enhanced band gap, ultraviolet-visible spectroscopy (UV-vis) was also used.

1. INTRODUCTION

Zirconium dioxide (ZrO_2) has attractive thermal, mechanical, electrical, and optical properties and has a high conductivity of oxygen ions, making it one of the imaginary ceramic materials. ZrO_2 also possesses better acid-base and heat stability. Under reducing atmospheres and photoirradiation, it remains stable [1]. Comparing ZrO_2 with other ceramic oxides (TiO_2, SiO_2, and Al_2O_3), ZrO_2 considered as the most favorable option for refractory material and catalyst assistance in isomerization and hydrogenation reactions because of these characteristics. Zirconia displays three polymorph phases under normal atmospheric pressure with increasing temperature: one is

the cubic phase (2370 °C-2750 °C, melting point), a tetragonal phase from 2370 °C to1175 °C, and a monoclinic phase from 1175 °C to ambient temperature. The change in temperature was determined when these phases were changed. In addition, as the pressure increases, ZrO_2 shows two more polymorphs at lower temperatures: orthorhombic-I and -II. The monoclinic phase, which is well-known for being extremely steady under standard atmospheric pressure and at room temperature, has no special uses. Because it develops when cooling out of the high-temperature tetragonal phase and is linked to 5% volume expansion with shear stress, which causes the ceramic materials to crack. The application of sintering zirconium dioxide material in modern ceramics was restricted by this significant problem. Fortunately, the same martensitic tetragonal to monoclinic transformation serves as the foundation for the technological and mechanical toughening of ceramic applications [2].

The high-temperature phases ZrO_2's cubic and tetragonal structures are helpful to use as electrolytes for solid oxide fuel cells and oxygen sensors that operate at lower temperatures. Stabilized ZrO_2 is used as a port liner for wire drawing dies and combustion engines because of its great strength, high fracture toughness, high hardness, and excellent resistance to heat shock. In addition, zirconia is used in many other areas of our lives, including dentistry [3], biomedicine [4], sensors [5], and catalysts [6]. Therefore, using zirconia material for most applications requires stabilizing cubic and tetragonal phases over a wider and higher temperature range. In order to produce a new material that is superior to either one alone, scientists are therefore trying to stabilize the tetragonal phase by changing the variables of the production method or by doping with other metal oxides [7].

It is vital to comprehend the formation process of these phases in order to execute the stabilization. The total number of anions that are linked to a cation is their coordination number. In monoclinic ZrO_2, which is stable at lower temperatures, Zr^{4+} cations have seven coordination numbers, whereas in tetragonal and cubic ZrO_2, they have eight. Due to the covalent link between Zr and O, monoclinic zirconia is demonstrated to be thermodynamically stable at lower temperatures, favoring a sevenfold coordination number (especially at ambient temperature). An increase in bulk zirconia's lattice oxygen ion vacancy concentration is the primary factor responsible for the stabilization of tetragonal and cubic structures at higher temperatures. ZrO_2's structure changes to a cubic or tetragonal one due to the bond between Zr^{4+} ions and oxygen ions. This allows for the accommodation of the heat-generated oxygen ions while preserving an effective number of coordination close to 7. Thus, the creation and interaction of oxygen ion vacancies with Zr^{4+} cations are primarily responsible for the stabilization of cubic and tetragonal structures at high temperatures. Under these conditions, the high temperatures result in an excess oxygen ion vacancy concentration; however, excess oxygen ions vacancies can also produce at lower temperatures in the surrounding atmosphere if the partial pressure of oxygen is dropped (for example, in a vacuum). When monoclinic or tetragonal zirconia is annealed at relatively lower temperatures and in atmospheres with low partial pressure of oxygen, either the monoclinic phase or the tetragonal phase transitions to the cubic phase. The generation of surplus oxygen ion vacancies in these conditions is thought to be the cause of this occurrence, and when exposed to air, the reverse transition is observed. This is brought about by oxygen ions diffusing into the zirconia lattice from the surrounding atmosphere. Given their stability

at high temperatures and low partial pressures of oxygen, it is evidence that oxygen ion vacancies are the only factor controlling the stabilization of cubic or tetragonal phases [8].

Trivalent cation doping of the zirconia lattice led to an increase in oxygen ion vacancies, stabilizing the tetragonal and monoclinic zirconia. Because of charge balancing, this method allows the generation of oxygen ion vacancies at room temperature. Ga^{3+}, Fe^{3+} (under-sized), Gd^{3+} and Y^{3+} (over-sized) cations stabilize the cubic and tetragonal phases at room temperature in a similar manner by generating oxygen ion vacancies. The doped large cations (Gd^{3+} and Y^{3+}) promote the eightfold coordination and allow the host Zr^{4+} cations to engage with oxygen ion vacancies. Therefore, through the higher temperature range, doping an appropriate number of oversized cations can successfully generate both tiny and large numbers of oxygen ion vacancies, associated with the host Zr^{4+} cations. Consequently, it is possible to stabilize both cubic and tetragonal zirconia at room temperature. On the other hand, because of the support sixfold coordination, doped zirconia with undersized cations (Ga^{3+} and Fe^{3+}) compete with the host Zr^{4+} cations for the oxygen ion vacancies. Consequently, only trace numbers of oxygen ion vacancies associated with the host Zr^{4+} cations may occur, even when doping a high number of undersized cations. Thus, only the tetragonal phase is stabilized at room temperature when undersized trivalent cations (Ga^{3+} and Fe^{3+}) are doped into the ZrO_2 lattice. At ambient temperature, the tetragonal phase is stabilized by the oxygen ion vacancies produced during the doping process. It was also demonstrated that the stabilization of cubic and tetragonal zirconia is solely controlled by the oxygen ion vacancies, with the doped metal cations having no appreciable impact on the process. Using a self-consistent tight-binding model allowed for this to be accomplished [9].

The main objective of this study is to examine the effects of varying the proportions of barium (under-sized bivalent cation impurities; ionic radii for Zr^{+4} is 0.160 nm and for Ba^{+2} is 0.134 nm) at different annealing temperatures on the creation of oxygen ion vacancies, which are associated with the host Zr^{4+} cations to stabilize the tetragonal phase.

2. MATERIALS AND METHODS

2.1 Materials

Sodium hydroxide (NaOH), extra pure barium chloride ($BaCl_2.2H_2O$), 98% extra pure zirconium oxychloride octahydrate ($ZrOCl_2.8H_2O$), and ethyl alcohol (CH_3CH_2OH). All of the chemicals were utilized without additional purification after being purchased from LABO CHEMIE PVT.LTD.

2.2 Synthesis of barium incorporated in zirconia lattice

After dissolving varying concentrations of barium chloride and zirconium chloride (x = 1%, 2%, 5%, 6%, 8%, and 10% Ba relative to Zr) in double-distilled water, the mixtures were rapidly stirred for 20 minutes with heating at 50 °C. Then sodium hydroxide (NaOH) will be added dropwise to the solution, and it will be continually stirred without heating for 20 minutes, or until a white gel forms. The gel will then cool for twenty minutes to room temperature. Ultimately, in order to get rid of any leftovers from the contact, it was cleaned several times in an ultrasonic cleaner using double-

distilled water and alcohol. After being dried at 60 °C for 24 hours, the gel was crushed and ground into a fine powder. With varied Ba and Zr ratios, the resultant powder is used to monitor the tetragonal phase development at different annealing temperatures between 400 °C and 1000 °C.

2.3 Characterization

A graphite monochromator (λ=1.54056 Å) and a Philips PW 1710 diffractometer with CuK_α radiation were used to obtain X-ray diffraction (XRD) at room temperature for both pure zirconia powder and Ba incorporated in the zirconia nanoparticles. The measuring angles ranged from 4° to 80°, and the scan rate was 0.06° per minute. Using an instrument with a standard error of ±1°, the STA PT/1600 simultaneous DSC-TGA was used. To perform thermogravimetric analysis (DSC), powder samples were heated to 1000 °C at a rate of 10 °C per minute in a crucible cell. With the NICOLET FTIR 6700 spectrometer, the transmittance (T) of the prepared samples was measured in the 4000-500 cm^{-1} wavenumber region using the KBr pellets method. By using a computerized UV-visible spectrophotometer model (JASCO V-770) with a 1 nm step, the absorbance (A) spectra were obtained for normal incidence at room temperature in the wavelength range of 200-900 nm. The surface morphology of the powder sample was examined using the JSM-T200 Jeol-Japan SEM device.

3. RESULTS

1.Structural (XRD) and thermal (DSC) data

According to XRD data, a typical tetragonal phase of ZrO_2 was obtained in samples of pure ZrO_2 in a narrow range of temperatures (annealed at 400-500 °C), at positions 2Θ = 30.3°, 35.1°, 50.3°, 60.1°, and 62.6°, matching with Card No. 01-079-1768 (Figure 1.a). However, the same phase appeared in samples containing 1% and 2% ratios of barite (Ba) in the zirconia lattice at 400-600 °C. After that, at temperatures between 700 and 800 °C, it starts to change to appear in a mixed phase of tetragonal and monoclinic phases. This mixed phase also appeared at 900 °C for a 2% Ba ratio, and this mixed phase eventually turned into a complete monoclinic phase (at positions 2Θ = 24.2°, 28.2°, 31.7°, 34.1°, 35.5°, 41.0°, 49.3°, 50.3°, 54.3°, 55.7°, and 60.1°, matching Card No. 37-1484, Figure 1.a), at both 900 and 1000 °C for a 1% ratio and only at 1000 °C for a 2% ratio as shown in Figure 1.b and Figure 1.c. For 5% and 6% Ba ratios, the tetragonal phase appeared at temperature ranging from 400 °C to 700 °C, the mixed phase at 800 to 900 °C, and the monoclinic phase at 1000 °C (Figure 1.d and Figure 1.e). But the tetragonal phase starts at 400 °C, continues to 800 °C for an 8% ratio (Figure 1.f), and continues to 900 °C for a 10% ratio (Figure 1.g). For an 8% ratio, the tetragonal phase starts to be mixed at 900 °C, after which it displays crystalline peaks linked to the monoclinic phase at 1000 °C. As a result, 10% Ba has the highest stabilization, so at 1000 °C, the mixed phase of tetragonal and monoclinic phases appeared. So, we can summarize that as follows: the tetragonal phase will stabilize to higher temperatures when the amount of barium incorporated into the zirconia lattice increases. Since different ratios of Ba added to zirconia at the same temperature result in different structures. The aim of this work is to determine the appropriate ratio for zirconia

to suit different purposes. In contrast to the previous study [7], which used varied Fe doping ratios in zirconia lattices at various annealing temperatures until arrive at 800 °C which considered the best temperature for the greatest ratio, Ba is used to stabilize the tetragonal phase at higher temperatures, which represent the ideal case.

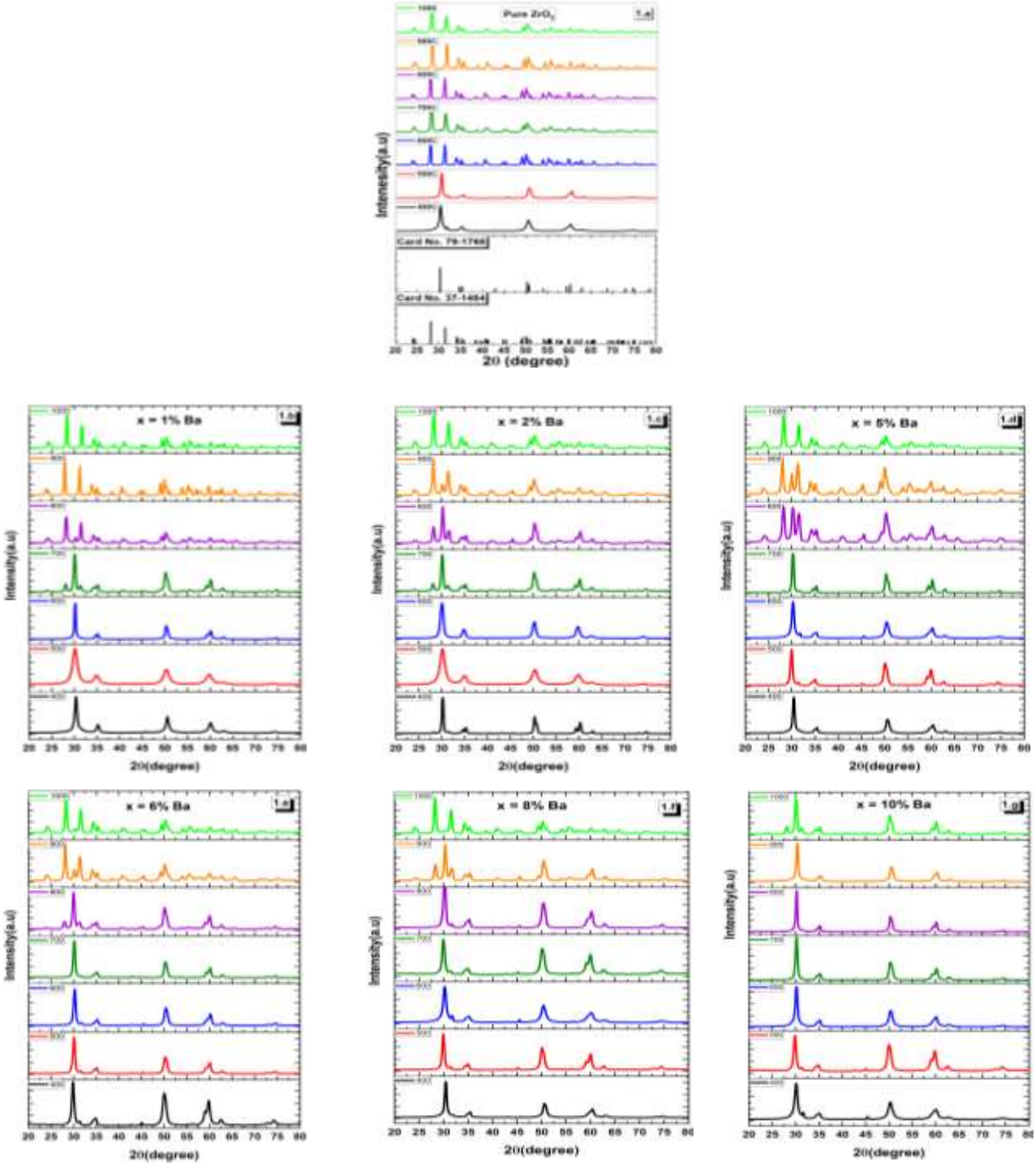

Figure 1. XRD pattern at different annealing temperatures for pure ZrO_2 and Ba-doped ZrO_2.

The lattice parameters for pure zirconia and zirconia doped with different Ba ratios were calculated and tabulated in Table 1. There is no significant change in lattice parameters for pure zirconia and zirconia doped with different Ba ratios, which indicates that the Ba ions were successfully incorporated into the zirconia lattice.

Table 1. Lattice parameters for pure zirconia and Ba-doped zirconia in the tetragonal and monoclinic phases.

Crystallite phase	**Lattice parameters**	**Doping concentration**						
		0%	1%	2%	5%	6%	8%	10%
Tetragonal	a	3.6000	3.5924	3.6156	3.6048	3.6110	3.6149	3.5961
	c	5.1674	5.1925	5.1746	5.1583	5.1735	5.1488	5.1760
	volume	66.97	66.93	67.01	67.03	67.28	67.46	66.65
Monoclinic	a	5.3053	5.3160	5.3143	5.3079	5.2951	5.3112	-
	b	5.2108	5.2104	5.2117	5.2142	5.2144	5.2059	-
	c	5.1355	5.1481	5.1464	5.1396	5.1464	5.1392	-
	β	99.26	99.13	99.22	99.17	99.18	99.16	-
	volume	140.12	140.79	140.70	140.40	140.40	140.28	-

The volume fraction of the tetragonal phase (V_t) was calculated by the first computing the average peak areas of the corresponding tetragonal $(101)_t$ plane and monoclinic planes $(-111)_m$, $(111)_m$, then applying the following formula [10] expressed in equation (1) (Figure 1.h), and the obtained data are listed in Table 2.

$$V_t = \frac{A(101)_t}{A(111)_m + A(-111)_m + A(101)_t} \quad (1)$$

Table 2 and Figure 2 show how the addition of Ba ions to the zirconia ions can stabilize the tetragonal phase at higher temperatures. The tetragonal phase appeared at 500 °C as a maximum temperature in pure zirconia, but the tetragonal phase continued up to 900 °C in the 10% Ba ratio.

The average crystallite size (D) for tetragonal zirconia was calculated based on the full width at half maximum intensity parallel to the (101) plane for the tetragonal phase and the (-111, 111) reflection for the monoclinic phase, with peak deconvolution for mixed phase samples, using the following Scherrer's equation [11]:

$$D = \frac{k\lambda}{\beta\cos\theta} \quad (2)$$

Where λ is the wavelength of CuK_α radiation, k is a minor factor with a value close to one, β is the full width at half maximum measured in radians, and θ is Bragg's diffraction angle.

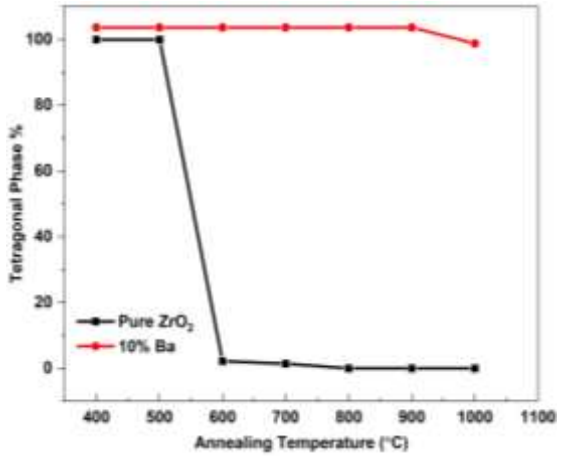

Figure 2. The influence of barium doping on the range of temperatures up to 1000 °C for the tetragonal phase of zirconia nanoparticles.

Table 2. The volume fraction for the tetragonal phase appeared at different annealing temperatures for pure zirconia and Ba-doped zirconia.

	Doping concentration	**Annealing Temperatures (°C)**						
		400 °C	500 °C	600 °C	700 °C	800 °C	900 °C	1000 °C
Phase ratio (%)	0%	T	T	T=2.2 M=97.8	T=1.4 M=98.6	M	M	M
	1%	T	T	T	T=88.3 M=11.7	T=2.7 M=97.3	M	M
	2%	T	T	T	T=67.9 M=32.1	T=72.2 M=27.8	T=10.8 M=89.2	M
	5%	T	T	T	T	T=55.7 M=44.3	T=46.7 M=53.3	M
	6%	T	T	T	T	T=92.0 M=8.0	T=17.0 M=83.0	M
	8%	T	T	T	T	T	T=76.9 M=23.1	M
	10%	T	T	T	T	T	T	T=95.1 M=4.9

The theoretical density (ρ) can be also estimated from the X-ray diffraction pattern using the formula [12]:

$$\rho = \frac{ZM}{N_A V} \tag{3}$$

Where Z is the number of molecules per unit cell (Z = 4 for the monoclinic phase and 2 for the tetragonal phase), V is the unit cell volume, N_A is Avogadro's number, and M is the molecular weight of the composition.

The strain (ε) in the packed structure can be calculated using the Williamson-Hall (W-H) formula [13]:

$$\varepsilon = \frac{\beta \, Cos(\theta)}{4} \tag{4}$$

Where β is the computed value for the most prominent crystallographic planes, the peak position is adjusted according to the strain value. This causes a change in the lattice constants and the estimated strain values.

The crystallite size is used, and the dislocation density (δ) can be calculated using the following equation [14]:

$$\delta = \frac{15\varepsilon}{aD} \tag{5}$$

The calculated grain size, dislocation density, density, and strain were listed in Table 3.

Table 3. The average grain size D (nm), dislocation density δ $(nm)^{-2}$, density ρ (g/cm^3), and strain ε (°) for pure and Ba-doped zirconia nanoparticles in the tetragonal and monoclinic phases.

Crystalline phase	**parameters**	**Doping concentrations**						
Tetragonal		**0%**	1%	2%	5%	6%	8%	10%
	D (nm)	10.2	16.6	16.18	15.69	14.15	13.51	11.84
	δ $(nm)^{-2}$	0.009	0.0036	0.0038	0.0036	0.0049	0.0054	0.0071
	Density (ρ)	6.90	6.152	6.219	6.219	6.517	6.275	6.865
	Strain ε (°)	0.003	0.002	0.002	0.002	0.003	0.003	0.003
	D (nm)	17.9	21.5	21.1	17.3	16.8	15.8	-
Monoclinic	δ $(nm)^{-2}$	0.003	0.001	0.002	0.003	0.003	0.003	-
	Density (ρ)	6.59	6.71	6.80	6.82	6.88	6.94	-
	Strain ε (°)	0.001	0.001	0.002	0.002	0.002	0.002	-

DSC analysis for pure zirconia and Ba-doped zirconia has curves that correspond to the creation of two phases, namely the tetragonal phase and the monoclinic phase, which confirmed the XRD results. As shown in Figure 3, the first peak emerged in the DSC curve, an endothermic peak around 150 °C, related to the loss of water. The second peak is an exothermic peak, centered around 450 °C for pure zirconia, and for all Ba ratios (1%, 2%, 6%, 8%, and 10%) are related to the tetragonal phase crystallization. The third peak, an exothermic peak is associated with the monoclinic phase, which appears at different locations for different Ba ratios (970-1200 °C). This discernible shift in the monoclinic phase's location towards higher temperatures for greater Ba ratios is caused by the stabilization of the tetragonal phase.

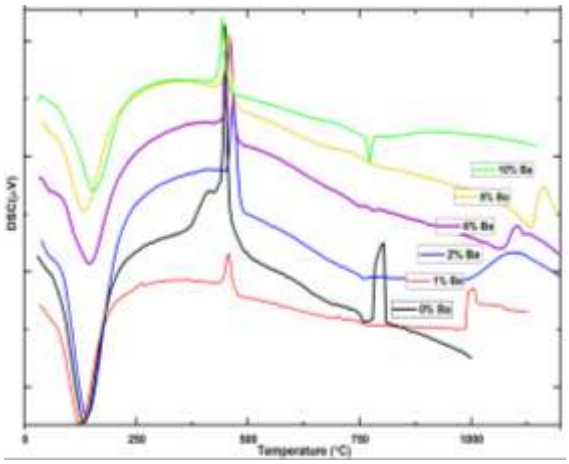

Figure 3. DSC curve for pure ZrO_2 and Ba- doped ZrO_2 nanostructures at different annealing temperatures.

3.2. phase composition analysis (FTIR)

FTIR spectra in the 500-4000 cm^{-1} wavenumber range for pure zirconia and different ratios of Ba present in the zirconia lattice in the tetragonal phase were acquired at 500 °C in order to identify the functional groups of the generated material, as depicted in Figure 4.

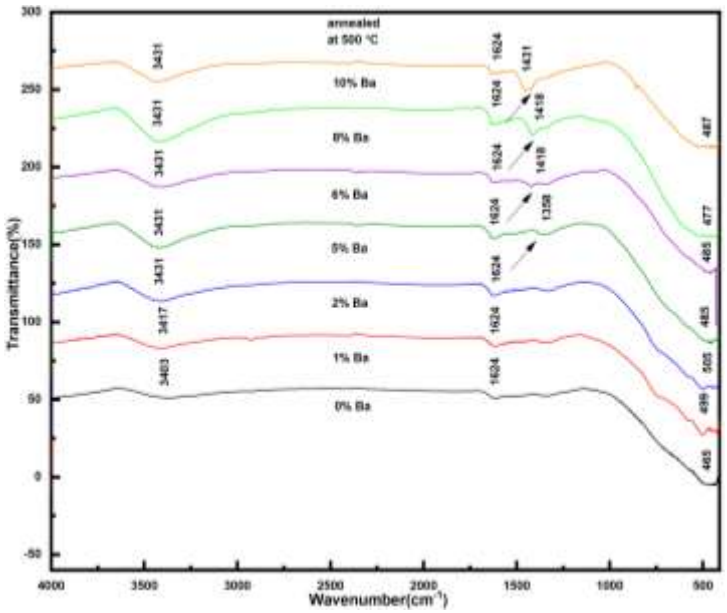

Figure 4. FTIR spectra for pure ZrO_2 and Ba doped ZrO_2.

.

The bands found in pure zirconia are ascribed to tetragonal stretching (t-Zr-O_2) at 465 cm^{-1}, O-H bending vibrations at 1624 cm^{-1}, and O-H stretching at 3403 cm^{-1} [15, 16]. FTIR spectra for ratios of 1% and 2% Ba exhibits behavior similar to that of pure zirconia, with a slight shift in peaks (peak locations of about 3020 cm^{-1},

1624 cm^{-1}, and 500 cm^{-1}) while no appearance of Ba because of the lower percentages. Nevertheless, when the Ba ratio is raised to 5%, 6%, 8%, and 10%, a new peak reflecting BaO emerges between 1350 cm^{-1} and 1420 cm^{-1} [17]. It can note that the height of BaO peak increases with increasing the Ba ratio (these ratios include enough Ba impurities to develop). It is confirmed that Ba was successfully absorbed into the zirconia lattice by the development of a peak that is linked with BaO. This result agrees with that obtained data from the XRD and DSC analysis.

3.3. optical analysis (Uv-visible spectroscopy)

The absorbance spectra of pure zirconium oxide and Ba, including zirconium oxide, at room temperature are shown in Figure 5 The figure clearly reveals that there is a characteristic peak for the BaO at approximately 270 nm in the small ratios and 280 nm in the big ratios as the highest light absorption, which is extremely close to the value stated in [18], indicating to the strong properties of Ba. According to the exported data, this peak vanished in the pure one and continued to emerge with the addition of Ba, enhancing as the Ba ratio increased. These data confirm the presence of Ba and indicate that barium was successfully incorporated into the zirconia lattice with superior properties to pure zirconium oxide. Furthermore, the data exported from all XRD, thermal testing (DSC), and FTIR spectra is perfectly consistent with these results. The Beer-Lambert law was employed to compute the absorption coefficient (α) in terms of the absorbance A [19].

$$\alpha = \frac{A}{cL} \tag{6}$$

Where c is the concentration of the suspension and L is the optical path length, and here is 1 cm.

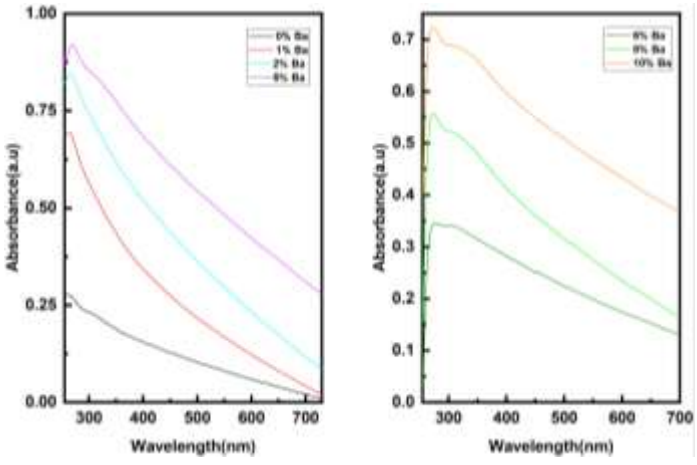

Figure 5. shows the absorbance spectra for pure ZrO_2 and Ba-doped ZrO_2 with different Ba-Zr ratios at selected annealing temperatures.

Tauc's law [20], which describes the relationship between incident photon energy and the absorption coefficient in the high absorption region of semiconductor materials, was used to calculate the optical band gap of the fabricated samples.

$$(\alpha h\nu)^2 = B(h\nu - E_g)^n \quad (7)$$

Where B is a probability constant, h is Planck's constant, and ν is the optical frequency, so that hν is the energy of the incident photon, E_g is the optical band gap energy, and n is an exponent whose value depends strongly on the type of the electronic transition. Therefore, n takes 1/2 for the direct transition and 2 for the indirect transition.

The optical behavior of pure zirconia and Ba incorporated in the zirconia lattice (Figure 6.a, and Figure 6.b) is unique in terms of improving the band gap structure when compared to the value obtained by E. Hemalatha et al. [21], who used the precipitation method for the preparation of pure ZrO_2 and Cu-doped ZrO_2 and obtained an energy gap of 5 eV for pure ZrO_2 and 4.5 eV as the optimal value for the highest ratio of Cu-doped ZrO_2 (15% Cu). Also, the results of C. Dhandapani et al. [22], who used the polymer-assisted sol-gel method in preparing ZrO_2 and Nd-doped ZrO_2, obtain 2.8 eV and 2.6 eV for pure ZrO_2 and Nd-doped ZrO_2, respectively. During our study of the optical properties of pure ZrO_2 and Ba-doped ZrO_2, we find that increasing the ratio of the Ba relative to Zr decreases the energy gap from 4.3 eV in pure ZrO_2 to 3.80 eV and 3.60 eV in the ratios 1% and 2% to a drastic decrease of 2.90 eV in the ratio 5%, and the improvement continues with increasing the ratio more to find it at 2.80 eV, 2.24 eV, and 2.10 eV for the large ratios 6%, 8%, and 10%. So, we have a range of energy gap values when the ratio changes, which can provide different types of applications.

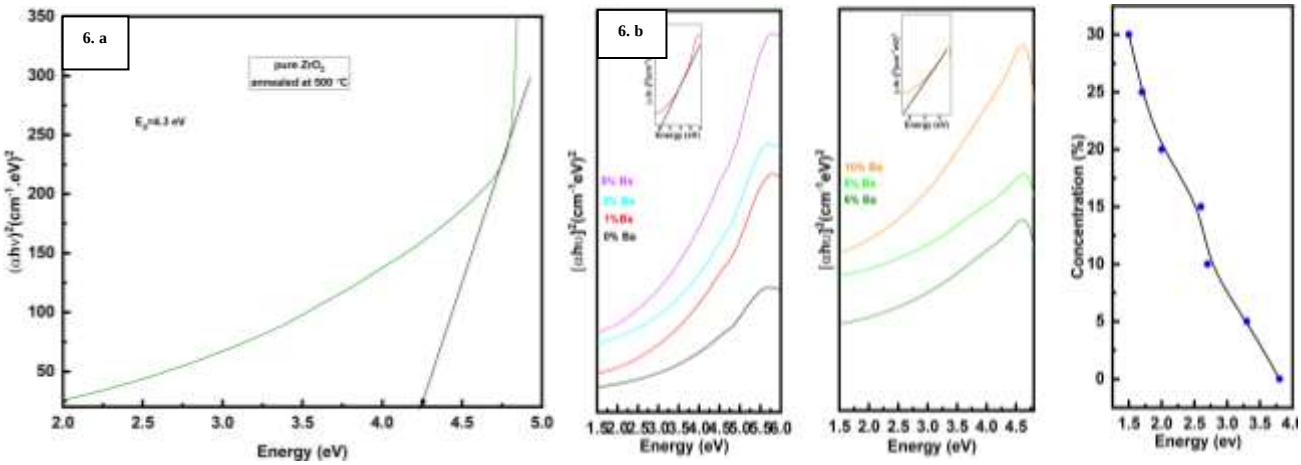

Figure 6. Tauc'c plot and optical band gap for pure ZrO_2 and Ba-doped ZrO_2 nanostructures.

3.4. morphological analysis (SEM)

In addition to the pure ZrO_2 sample, three various Ba ratios (5%, 8%, and 10%) were chosen for the study of the morphology of the generated structure under a scanning electron microscope, as shown in Figure 7. The investigation demonstrates that the surface morphology of pure ZrO_2 samples resembles a coral shape, matching the data in [23]. And for the Ba-doped ZrO_2 ratios, there is an agglomeration in the form of whiskers, as stated by Zhe et al. [24], which increases with increasing Ba ratio.

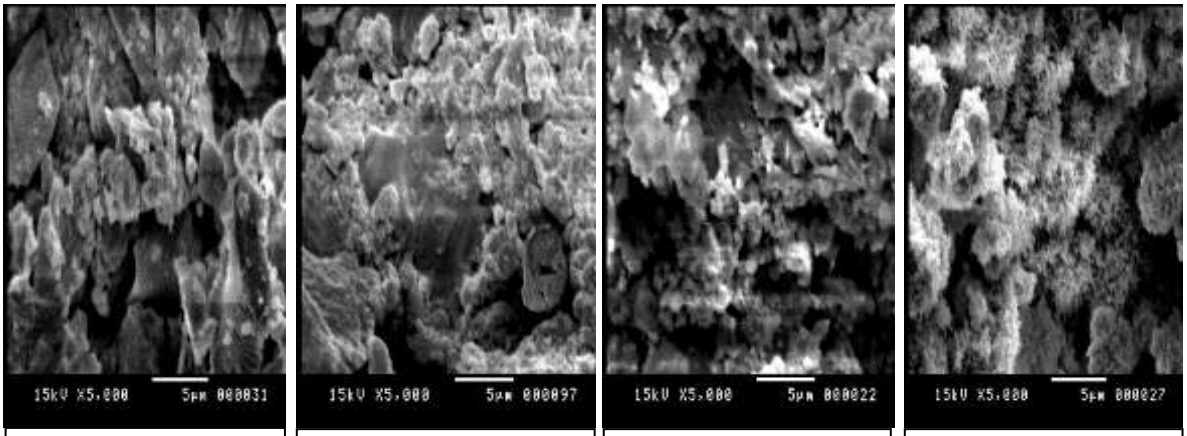

Figure 7. SEM images for pure ZrO_2 and Ba-doped ZrO_2.

4. CONCLUSION

According to the study of the influence of different percentages of Ba relative to Zr on the creation of the tetragonal phase of zirconia, we can infer that we have a wide range of applications at different annealing temperatures depending on the suitable ratio. These findings are based on XRD data, indicating that as the Ba ratio increased, the tetragonal phase continued up to higher annealing temperatures (1% gives the tetragonal phase at 400 °C up to 600 °C, but 10% starts the tetragonal phase at 400 °C up to 900 °C). The DSC analysis confirmed the stabilization in which the exothermic peak related to the crystallization of the monoclinic phase shifts towards higher temperatures (meaning that the tetragonal phase is continued to higher temperatures). FTIR data confirm the successful synthesize of pure zirconia and Ba-doped zirconia. The signal connected to Ba appears in small Ba ratios and becomes stronger as the ratio of Ba increases in the FTIR data. The optical band gap decreased from 4.30 eV in pure t-ZrO_2 to 3.80 eV in 1% Ba and 2.10 eV in 10% Ba. The SEM images for selected ratios confirm the existence and increase of Ba in the zirconia lattice at different temperatures for different ratios. So, we may choose the right utilization ratio based on the desired application concerning the (temperature and band gap).

REFERENCES

[1] A. Bhujel, B. Sapkota, R. L. Aryal, B. R. Poudel, S. Bhattarai, S. K. Gautam, Insight of precursor concentration, particle size and band gap of zirconia nanoparticles synthesized by co-precipitation method, Bibechana, 18 (٢٠٢١) 1.

[2] S. Shukla, S. Seal, Mechanisms of room temperature metastable tetragonal phase stabilization in zirconia, Int. Mater. Rev., 50 (٢٠٠٥) 45.

[3] C. Hu, J. Sun, C. Long, L. Wu, C. Zhou, X. Zhang, Synthesis of nano zirconium oxide and its application in dentistry, Nanotechnol Rev., 8 (2019) 396.

[4] A. V. Shevchenko, E. V. Dudnik, A. K. Ruban, V. P. Red'ko, V. M. Vereschaka, L. M. Lopato, Nanocrystalline powders based on ZrO_2 for biomedical applications and power engineering, Powder Metall. Met. Ceram., 41 (2002) 558.
[5] L. Zhian, X. Jianzhong, X. Feng, Y. Yifan, Preparation and characterization of zirconia oxygen sensors, J. Wuhan Univ. Technol.-Mater. Sci. Ed., 22 (2007) 612.
[6] S. Chen, A. Tennakoon, K. You, A. L. Paterson, R. Yappert, S. Alayoglu, L. Fang, X. Wu, T. Y. Zhao, M. P. Lapak, M. Saravanan, R. A. Hackler, Y. Wang, L. Qi, M. Delferro, T. Li, B. Lee, B. Peters, K. R. Poeppelmeier, S. C. Ammal, C. R. Bowers, F. A. Perras, A. Heyden, A. D. Sadow, W. Huang, Ultrasmall amorphous zirconia nanoparticles catalyse polyolefin hydrogenolysis, Nat. Catal., 6 (2023) 161.
[7] A. Abu El-Fadl, A. M. Eltokhey, A. A. Abu-Sehly, A. A. Abozeed, Stabilization of tetragonal phase of nanostructured Fe_x/ZrO_2 system ($0\leq x\leq 25$) prepared by modified sol-gel method, Phys. Scr., 97 (2022) 1.
[8] N. Mommer, T. Lee, J. A. Gardner, Stability of monoclinic and tetragonal zirconia at low oxygen partial pressure. J. Mater. Res., 15 (2000) 377.
[9] P. Li, I.-W. Chen, J. E. Penner-Hahn, Effect of Dopants on Zirconia Stabilization-An X-ray Absorption Study: I, Trivalent Dopants, J. Am. Ceram. Soc., 77 (1994)118.
[10] A. C. Bose, R. Ramamoorthy, S. Ramasamy, Formability of metastable tetragonal solid solution in nanocrystalline $NiO-ZrO_2$ powders. Mater. Lett., 44 (2000) 203.
[11] S. Gutzov, J. Ponahlo, C. L. Lengauer, A. Beran, Phase characterization of precipitated zirconia, J. Am. Ceram. Soc., 77 (1994) 1649.
[12] A. Abu El-Fadl, M. Almokhtar, A. M. Nashaat, Fabrication and analysis of the structural phase transition of ZrO_2 nanoparticles using modified facile sol-gel route, Phase Trans., 92 (2019) 36.
[13] A. A. El-Fadl, M. A. M. Hussien, A. S. Soltan, A. Abu-Sehly, Structure, optical and visible-light photocatalytic performance of $Mo_{1-x}Co_xS_2$ ($0\leq x\leq 0.1$) nanoparticles synthesized by facile hydrothermal method for methylene blue dye degradation, Dig. J. Nanomater. Bios., 19 (2024) 65.
[14] S. Chander, M. S. Dhaka, Impact of thermal annealing on physical properties of vacuum evaporated polycrystalline CdTe thin films for solar cell applications, Phys. E: Low-Dimens. Syst. Nanostructures., 80, (2016) 62.
[15] S. Zinatloo-Ajabshir, M. Salavati-Niasari, Zirconia Nanostructures: Novel Facile Surfactant- Free Preparation and Characterization, Int. J. Appl. Ceram. Technol., 13 (2016) 108.
[16] P. P. Khirade, Structural, microstructural and magnetic properties of sol-gel-synthesized novel $BaZrO_3$-$CoFe_2O_4$ nanocomposite, J. Nanostruc. Chem., 9 (2019) 163.
[17] J. Swain, A. Priyadarshini, S. Hajra, S. Panda, J. Panda, R. Samantaray, Y. Yamauchi, M. Han, H. J. Kim, R. Sahu, Photocatalytic dye degradation by $BaTiO_3$/zeolitic imidazolate framework composite, J. Alloys Compd., 965 (2023) 1.
[18] M. A. Ansari, N. Jahan, Structural and optical properties of BaO nanoparticles synthesized by facile Co-precipitation method. Mater. Highl., 2 (2021) 23.

[19] A. Abu El-Fadl, A. M. Eltokhey, A. A. Abu-Sehley, H. M. El-Attar, Fabrication and analysis of the structural phase transition of ZrO_2 nanoparticles using modified facile sol-gel route, Phase Trans., 92 (2019) 36.
[20] A. Abu El-Fadl, M. Almokhtar, A. M. Nashaat, Synthesis, structural, optical, and magnetic properties of $ZnCr_{2-x}Fe_xO_4$ ($0 \leq x \leq 0.8$) nanoparticles, Jpn. J. Appl. Phys., 57 (2018) 1.
[21] E. Hemalatha, N. Gopalakrishnan, Gas sensing performances of pure and Cu-doped ZrO_2 nano structures, Appl. Phys. A, 125 (2019) 1.
[22] C. Dhandapani, R. Narayanasamy, S. N. Karthick, K. V. Hemalatha, S. Selvamc, P. Hemalatha, M. S. kumar, S. D. Kirupha, H. Kim, Drastic photocatalytic degradation of methylene blue dye by neodymium doped zirconium oxide as photocatalyst under visible light irradiation, Optik, 127, (2016) 10288.
[23] M. R. H. Siddiquia, A. I. Al-Wassil, A. M. Al-Otaibi, R. M. Mahfouz, Effects of precursor on the morphology and size of ZrO_2 nanoparticles, synthesized by sol-gel method in non-aqueous medium, Mater. Res., 15, (2012) 986.
[24] Z. Qiao, S. Li, Y. Li, J. Wang, Properties of barium zirconate sintered from different barium and zirconium sources, Ceram. Int., 47 (2021) 31194.